Regenerative Engineering and Translational Medicine (2024) 10:205–219
https://doi.org/10.1007/s40883-023-00312-2

ORIGINAL RESEARCH

Ultrasound-Derived Mechanical Stimulation of Alginate Hydrogels for Bone Repair: an In Vitro Study

Fayekah Assanah[1,2] · Hanna Anderson[1,2] · Kevin Grassie[1,2] · Lakshmi Nair[1,2,3] · Yusuf Khan[1,2,3]

Received: 5 March 2023 / Revised: 2 June 2023 / Accepted: 22 June 2023 / Published online: 18 July 2023

Abstract

Purpose Cell therapy is a new and evolving treatment for large-scale bone defects. Here, we describe a novel approach that combines hydrogel-based cell therapy with low-intensity pulsed ultrasound (LIPUS), an FDA-approved treatment for fracture repair.

Methods Bone marrow–derived stromal cells (BMSCs) were encapsulated in RGD-peptide-coupled alginate hydrogels and mechanically stimulated using LIPUS-derived acoustic radiation force (ARF).

Results Mechanical analysis of alginate hydrogels revealed a dependence on either alginate concentration or cross-linker concentration, revealing different ways to adjust the mechanical properties of the hydrogel. An optimal alginate and cross-linker concentration were found that allowed both robust cell proliferation and hydrogel mechanical stability. Cell proliferation was inversely proportional to hydrogel stiffness, suggesting that stiffer hydrogels were preventing full cell spreading and migration within the hydrogel. Cells encapsulated in hydrogels of optimal stiffness responded immediately after the onset of ARF by upregulating calcium, and shortly after upregulating cyclooxygenase-2 and prostaglandin E2, and later forming mineralized tissue in culture. Interestingly, cells seeded on top of hydrogels did not demonstrate the same calcium flux as encapsulated cells, suggesting that encapsulating the cells provided an additional mechanical stimulus. COX-2 and PGE_2 data from cells encapsulated in hydrogels with no ARF showed a similar response to encapsulation alone.

Conclusion These studies support the idea of combining cell therapy with LIPUS-derived ARF to enhance mineralized tissue formation.

Lay Summary Ultrasound has been a tool available to clinicians for a long time, and for a wide range of applications, including bone repair. Here, we show that it can stimulate stem cells that have been encapsulated in hydrogels to differentiate into bone cells through mechanical stimulation. This work would allow a clinician to implant stem cells into a large bone defect and stimulate them using ultrasound to differentiate into bone cells and help these large defects heal more quickly. This stimulation would be done transdermally and non-invasively, allowing the defect to heal with minimal intervention.

Keywords Hydrogel · Alginate · Cell therapy · Acoustic radiation force · Ultrasound

Introduction

Each year there are millions of orthopedic surgeries done that use bone grafts to heal large-scale bone defects that can result in non-unions or delayed unions [1, 2], costing approximately $2.5 billion [2–4]. Traditional approaches to large-scale bone repair include autografts, allografts, and bone graft substitutes. Autograft, tissue harvested and reimplanted in the same individual, continues to be the gold standard for large-scale bone defects because the patient-specific tissue mitigates immuno-rejection or other complications [5, 6], but introduces supply limitations, post-operative pain, and donor-site morbidity. Allograft, bone transplanted from a

✉ Yusuf Khan
ykhan@uchc.edu

1 Department of Biomedical Engineering, University of Connecticut, 260 Glenbrook Ave, Storrs, CT 06269-3247, USA

2 Connecticut Convergence Institute for Translation in Regenerative Engineering, UCONN Health, 263 Farmington Ave, CT 06030 Farmington, USA

3 Department of Orthopedic Surgery, UCONN Health, 263 Farmington Ave, Farmington, CT 06030, USA

cadaver, provides an important and popular alternative but has a risk of disease transmission or immune rejection [7, 8] and tends to be less effective at healing large, critical-size defects. With such limitations, alternative strategies are warranted. Regenerative engineering has emerged as a viable pathway for novel solutions to traditional approaches and typically involves the use of cells, scaffolds, and signaling molecules to help regenerate tissues that do not heal on their own [9–14]. Here, we describe a treatment strategy that incorporates clinical therapies currently in practice with novel regenerative strategies to heal large-scale bone defects.

The approach described herein combines hydrogel-based cell therapy with low-intensity pulsed ultrasound (LIPUS), an FDA-approved treatment for fracture repair. On its own, cell therapy describes the manipulation of cells outside of the body and subsequent implantation [15, 16] and has been used to treat a range of ailments including musculoskeletal disorders [13, 16, 17]. In many instances, cells are combined with hydrogels that serve to retain the cells after implantation at the injury site to encourage healing [14, 18, 19] LIPUS has been used extensively as a tool to assist with delayed- and non-union fracture repair for several decades. Its low intensity does not produce any ambient heat and it can be applied safely for extended periods of time. It has been shown to produce a very low-level mechanical force [18, 19] that may contribute to its utility as it is well established that mechanical strain and fluid shear can impact cellular responses including osteoblastic behavior and stem cell differentiation [20–24]. Other studies have also indicated that the mechanical properties of a substrate can determine the fate of the stem cells [25–28]. However, very few studies have sought to combine both externally applied forces and substrate mechanical properties simultaneously to impact cell behavior.

Here, we describe an approach in which cells could be delivered to bony defects via cell-laden hydrogels and then mechanically loaded using transdermally applied LIPUS that delivers a low-intensity acoustic radiation force (ARF). This approach allows the implanted cells to be mechanically stimulated, which has been documented to encourage both cell differentiation and eventual mineralization while in situ [18, 19, 29] but without mechanically destabilizing the unstable bone defect, allowing for the continuous mechanical stimulation of the implanted cells without mechanically disrupting the healing environment. Thus far, we have evaluated this approach using type I collagen hydrogels that have been loaded with either osteoblast precursors (MC3T3 cells) [18, 19] or bone marrow–derived stromal cells (BMSCs) [29] and found that cell behavior can be modulated by modifying the stiffness of the hydrogel and/or the intensity of the ARF. We have also shown that when the same type I collagen hydrogels are loaded with BMSCs and implanted into mouse calvarial defects, the defects heal faster and more completely when stimulated transdermally with ARF while they heal [29]. Thus, ultrasound was translated as a physical force to collagen hydrogels, and the impact of this force on the encapsulated cells was modulated by adjusting the hydrogel stiffness, the ARF intensity, or both [18, 19, 29].

Here, we sought to expand this approach to a different hydrogel system that is widely utilized and reported in the literature as a tool for hydrogel-based cell delivery. Alginate is biocompatible and biodegradable, has tunable mechanical properties, and has a more expansive range of mechanical properties which, given the importance of the mechanical loading on implanted cells, would increase the control over how the cells were loaded. To accomplish this, we have developed tissue mimetics of peptide-coupled alginate hydrogels and evaluated the behavior of encapsulated BMSCs in response to varied hydrogel stiffness and ARF intensities. Specifically, we investigated whether the ultrasound-generated physical forces within a hydrogel can stimulate encapsulated BMSCs to form mineralized tissue, in vitro by modifying (1) the stiffness of the hydrogel and (2) the intensity of the ARF, which subsequently alter the physical forces that the encapsulated BMSCs experience. We hypothesized that the appropriate combination of these parameters will translate into appropriate physical loading to upregulate bone markers and tissue mineralization, and that this approach is viable using the alginate hydrogel system. We determined an optimal combination of hydrogel stiffness/ARF intensity that initiated an upregulation of intracellular calcium concentration ($[Ca^{2+}]_i$), prostaglandin E_2 (PGE_2), and cyclooxygenase-2 (COX-2) through imaging, ELISA, and gene expression, respectively (all well-established precursors of stem cell differentiation and bone formation), and eventual mineralization of stem cell–encapsulated hydrogels through Alizarin Red staining (ARS) of the hydrogels. Studying these parameters thoroughly will better inform clinical applications regarding treatment regimens and/or duration of treatment.

Materials and Methods

Fabrication of Alginate Hydrogels

Alginate hydrogels were made using two different methods: one for rheological testing and one for in vitro cell studies. For rheology studies, alginate solutions (Millipore Sigma, Burlington, MA) of varying concentrations (0.25%, 0.5%, 1%, and 2%) (w/V) were made by dissolving the alginate in deionized water. Separately, varying concentrations of the cross-linking agent calcium chloride ($CaCl_2$, Millipore Sigma, Burlington, MA) (2, 5, and 10 mM) were made. Ten milliliters of the alginate solution was pipetted into a 10 cm Petri dish, to which $CaCl_2$ solution was slowly added and

allowed to sit for 2 h, ensuring adequate diffusion of calcium ions for complete cross-linking of the alginate monomers for gelation.

For cell encapsulation studies, peptide-coupled alginate from NovaMatrix (Norway) (LVM GRGDSP) was used with peptide sequence GRGDSP (Gly-Arg-Gly-Asp-Ser-Pro) to enhance the biocompatibility of the alginate hydrogels. It has been demonstrated that adding the peptide sequence does not alter mechanical properties [30] so correlations between the mechanical properties of one formulation and stiffness-dependent cell behavior in the other are valid. To encapsulate cells, a cell suspension was added (cell density of 1 million cells/mL) to the alginate solution, which was made with complete cell culture media containing α-MEM and supplemented with 10% fetal bovine serum (FBS) and 1% Penn/Strep (P/S). For all cell studies, 500 µL of the alginate solution was used (except for the intracellular calcium studies, as explained below). To make the individual hydrogels, transwell inserts were filled with 500 µL of cell/hydrogel suspension, and then $CaCl_2$ was slowly added on top of the alginate solution in the transwell insert. The well surrounding the transwell was also filled with 10 mM $CaCl_2$ to submerge the insert completely, to make sure the alginate solution was exposed to $CaCl_2$ similar to the method of gel fabrication for rheological testing. The bottom permeable membrane of the transwell (with 0.4 µm pore size) permitted the free diffusion of calcium ions from the surrounding well into the cell-alginate solution to cross-link the hydrogels. The transwells were placed on a rocker (to ensure free calcium ions are available to cross-link the alginate solution) at 37 °C for 2 h to ensure adequate diffusion of calcium ions throughout the alginate solution to form a homogeneous structure. After 2 h, the alginate hydrogel was cross-linked and the $CaCl_2$ was removed, and the hydrogels were rinsed with PBS and submerged with complete media in the transwells. This was done to ensure that there were no free calcium ions. Figure 1 shows the experimental setup with the orientation of the ultrasound transducer and the hydrogels in the 12 mm transwell.

Acoustic Radiation Force Application

For all cell studies, ARF was applied to cell-hydrogel constructs 24 h after seeding/encapsulation. Cell-hydrogel constructs that were formed in 12 mm insert transwells were exposed to ARF using a 6.35 mm diameter, 1 MHz unfocused immersion transducer (TLC Ultrasound Inc., New Milford, CT). ARF intensities (100, 150, and 300 mW/cm^2) were generated using a waveform generator (Agilent Technologies, Santa Clara, CA), and an ENI RF amplifier (Bell Electronics, Renton, WA) that produced a continuous signal with a 1 MHz carrier frequency (Fig. 1). The head of the transducer was positioned approximately 2 mm from the cell-hydrogel constructs and was submerged in cell culture media to minimize attenuation. Constructs were treated with ARF for 20 min/day, 5 days/week, for up to 21 days. This ARF treatment regimen was based on the FDA-approved method for treating fractures which includes a 20-min treatment per day of the fracture area using low-intensity ultrasound, with the guideline that local heating does not exceed 1°C. In our studies, the highest intensity used here

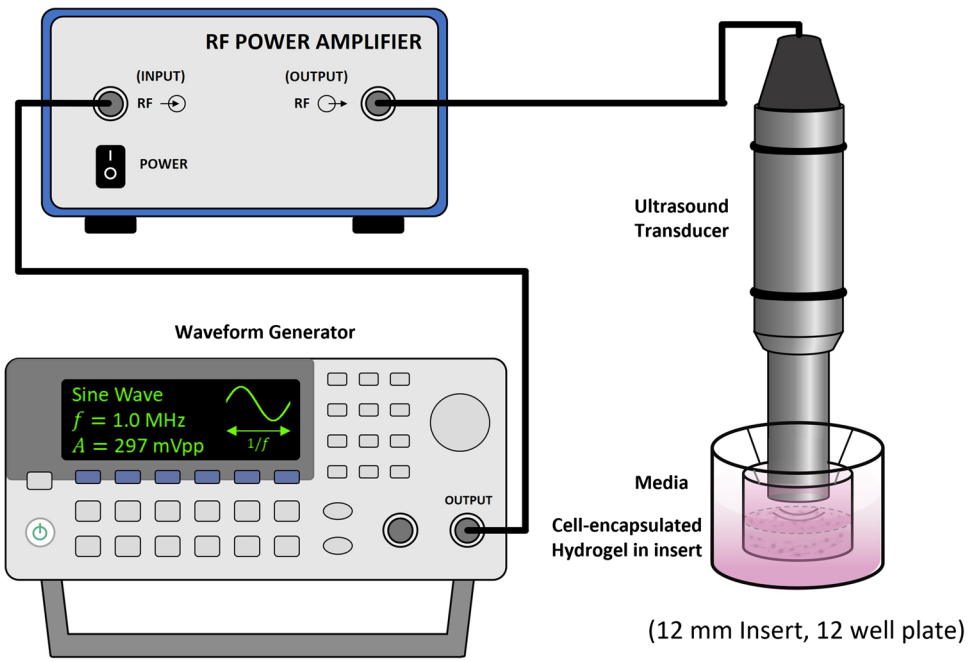

Fig. 1 Experimental setup for ARF application to cell-laden alginate hydrogels. Cell/hydrogel constructs were made in 12-mm inserts in 12-mm well plates. The transducer was placed directly above the alginate hydrogels in the insert and submerged in media. Adapted from [29]

(300mW/cm^2) did not raise the local temperature after 20 min of application (unpublished data).

Mechanical Properties of Alginate Hydrogels

For rheology studies, hydrogels were made according to the protocol above ("Fabrication of Alginate Hydrogels") using alginate solutions of varying concentrations and $CaCl_2$ of various concentrations. Specifically, smaller 12 mm alginate hydrogel discs were cut from the 10 cm alginate hydrogel, after gelation, to fit the 12 mm diameter surface of the parallel plate rheometer (Discovery Hybrid Rheometer, TA Instruments). Hydrogels for the rheology testing were tested wet, were acellular, and had not been exposed to ultrasound. A range of hydrogel stiffnesses were made by changing either (1) the $CaCl_2$ solution concentration (2 mM, 5 mM, and 10 mM) while maintaining a 2% alginate concentration or (2) the alginate concentration (0.01%, 0.1%, 0.25%, 0.5%, 1%, and 2%) (w/V) while maintaining a 10 mM $CaCl_2$ solution. The mechanical properties (storage and loss modulus) of the hydrogels were measured through frequency sweeps under uniaxial loading with a maximum strain of 1% within a 10% linear viscoelastic region.

Bone Marrow Stromal Cell Isolation

For all cell studies, BMSCs were isolated from the bone marrow of tibiae and femurs of male and female wild-type (WT) CD1 mice, aged 8–10 weeks by flushing with Dulbecco's Modified Eagle Medium (D-MEM) supplemented with 10% FBS and 1% P/S. Flushed marrow was plated after cell harvest (day 0) in a 10 cm tissue culture dish and cultured for 4 days to get an adherent and homogeneous cell population. Dead or floating cells were discarded on day 4. On day 7, 85% of confluent cultures were rinsed with sterile PBS and lifted. Cells were then encapsulated in alginate hydrogels at a density of 1×10^6/ml as described above.

To confirm the stemness of the BMSCs harvested for our studies, after 7 days on TCP, flow cytometry was performed to determine if $CD44^+$, $CD73^+$, $CD90^+$, and $CD105^+$ (well-established stem cell markers) were present and hematopoietic and endothelial markers ($CD\ 45^-$, $CD31^-$) were absent. Harvested and cultured BMSCs were gated for the negative markers.

Cell Viability of Bone Marrow Stromal Cells in Different Alginate Hydrogels

To determine the effects of alginate concentration and stiffness on the viability of BMSCs, we utilized MTS (Promega, Madison, WI) and Live/Dead assays (Millipore Sigma, Burlington, MA). BMSCs were encapsulated in 500 µL of alginate hydrogel at a density of 1 million cells per 1 mL of the alginate hydrogel (0.25, 0.5, and 1%) using the transwell method, then maintained in 37 °C, αMEM media (10% FBS, 1% P/S) for up to 5 days. BMSCs cultured on TCP (5×10^5 cells/well) served as the 2D control. On day 5, the viability of the encapsulated BMSCs was evaluated using MTS and Live/Dead assays. MTS assay protocol was performed, and all reagents were made according to the manufacturer's protocol. First, a standard curve was made correlating the absorbance of the formazan dye (in the MTS reagent) at 490 nm to known cell number on TCP. Next, the cell-encapsulated hydrogels were transferred from the transwells into a 24-well culture plate. Then, hydrogels and TCP samples were incubated with the MTS reagents for 2 h in the incubator for the color to develop. The 2-h incubation period was kept constant for all hydrogels and TCP samples. After color development, the solution was extracted from the hydrogels and read in a spectrophotometer using a wavelength of 490 nm. Finally, the standard graph was used to determine the total number of cells.

Alizarin Red Staining (ARS) for Mineralization

To evaluate mineralization within the hydrogels, 0.5% alginate hydrogels (500 µL) were cross-linked with 10 mM $CaCl_2$ solution ($n = 4$) and exposed to three different ARS intensities (100, 150, and 300 mW/cm^2) for 20 min/day, 5 days/week, for up to 21 days. All ARS-treated hydrogels were stained on day 21 following the ARS manufacturer's protocol. Briefly, all samples were fixed using 4% paraformaldehyde (PFA) for 15 min, stained with 40 nM Alizarin Red stain (ARS) (Millipore Sigma, Burlington, MA) in water (pH 4.2) for 20 min, and washed with deionized water several times to eliminate any unbound stain. Positive staining was imaged through a dissection microscope to obtain qualitative macroscopic images of the mineralization [29].

To extract and quantify ARS, the cultures were treated with 10% cetylpyridinium chloride (CPC) (Millipore Sigma, Burlington, MA) solution, and the resulting purple solution was collected and read using a spectrophotometer (540–570 nm). The optical density of the respective control samples with neither cells nor ARF was subtracted as background from each relevant group.

Intracellular Calcium Quantification

Fluo-4 is an acetoxymethyl (AM) ester that enables a dye to easily cross the cell membrane and, once inside the cell, allows calcium ions to bind to the free dye in the cytosol. For measuring intracellular calcium concentration, we used BMSC-encapsulated, 0.5% alginate hydrogels cross-linked with 10 mM $CaCl_2$ solution and exposed to an ARF intensity of 300 mW/cm^2. This tool was used to image fluxes in the concentration of calcium inside

BMSCs as a measure of the impact our system of ARF and hydrogels had on $[Ca^{2+}]_i$. To understand the dynamics of $[Ca^{2+}]_i$ in BMSCs when exposed to ARF, two scenarios were tested: (1) BMSCs on top of hydrogels and (2) BMSCs encapsulated in hydrogels. For cells on top of the hydrogel, 300×10^3 BMSCs were plated on top of 150 µL of 0.5% alginate hydrogel in plasma-coated fluoro-dish, separately, as described before. For encapsulated cells, BMSCs (cell density of 1 million cells/ mL) were encapsulated within 150 µL of 0.5% alginates in plasma-coated fluoro-dish, separately. The smaller hydrogel volume was used to maximize image clarity in the fluoro-dish but otherwise was the same as all other experiments. All cultures were maintained in complete media in the incubator for 2 days to allow cell attachment to the hydrogel. After 2 days, the cell-hydrogel constructs were washed three times with Hanks' Balanced Salt Solution (HBSS) (without calcium and magnesium) and then incubated in 5 µM Fluo-4 AM (Thermo Fisher Scientific, Waltham, MA), and 0.02 % Pluronic detergent (Thermo Fisher Scientific, Waltham, MA) in phenol-free Opti MEM supplemented with 1% FBS for 40 min. After incubation with the stain, cell-hydrogel constructs were washed three times with HBSS and then allowed a de-esterification process in HBSS for additional 30 min, after which the constructs were loaded with imaging media (phenol-free Opti MEM supplemented with 1% FBS) to ensure there were no free calcium ions in the imaging media to confound calcium ion imaging.

The $[Ca^{2+}]_i$ of the BMSCs was visualized and recorded in real-time using a Leica epifluorescence microscope (Leica DMi8) and camera (Leica DFC7000 T). The transducer was submerged in media and placed directly above the cell-hydrogel construct. All images were obtained at 10× objective using excitation and emission wavelengths of 488 nm and 515 nm, respectively. For all experiments, the ARF was switched OFF for the first 30s to obtain a baseline reading of $[Ca^{2+}]_i$, and then turned ON to a spatial intensity of 300 mW/cm^2 for a duration of 1 min then OFF again while another 30s of imaging was collected to observe the post-stimulation response of the cells. The average fluorescent intensity for each cell in the plane of view was analyzed using MetaMorph (Molecular Devices LLC, San Jose, CA) image analysis software. Relative calcium intensity per cell was plotted over time for each of the conditions using the formula: $\Delta F/F$, where F = average fluorescent intensity for unstimulated cells. Experiments were carried out 10 times (10 distinct hydrogels) with at least four separate regions of interest imaged for each hydrogel. A wait time of 5 min was added between each region of interest to ensure that the mechanical effects of the previous ultrasound were not compounded.

Prostaglandin E_2 (PGE_2) and Cyclooxygenase-2 (COX-2) Expression Quantification

Real-time quantitative reverse transcription–polymerase chain reaction (RT-PCR) was performed for COX-2 via TaqMan gene expression assays (Thermo Fisher Scientific, Waltham, MA). BMSCs were encapsulated in 500 µL of 0.5% alginate hydrogel (cell density of 1 million cells /mL) and formed in 12-mm insert transwells as described before. After 24 h, the cell-hydrogel constructs were exposed to one session of ARF with an ultrasound intensity of 300 mW/cm^2 for 20 min. The control groups did not receive ARF. Cell-laden hydrogels were then incubated for 1 h after ARF exposure and the media was collected for PGE_2 analysis (see below). Alginate hydrogels were then rinsed with PBS and digested with 0.3 M trisodium citrate (Thermo Fisher Scientific, Waltham, MA), to permit cells to be isolated for COX-2 analysis. Three hydrogels were combined for each replicate for a total of $n = 3$. Total RNA was extracted from cells within gels with RNeasy Mini (Qiagen, Valencia, CA). cDNA was then synthesized using Clontech EcoDry Premix (Double Primed) reverse transcription kit (Clontech, Mountain View, CA). Amplification curves for the experimental and the control genes were recorded over the iQ5 RT-PCR machine (BioRad, Valencia, CA), and the relative gene levels between samples were quantified. Data were calculated via the delta-delta Ct method and normalized to housekeeping gene GAPDH, relative to the control sample. Experiments were carried out for three biological repeats.

PGE_2 released into the media collected from each sample was quantified using a competitive enzyme immunoassay kit (R&D Systems, Minneapolis, MN) following the manufacturer's protocol. Briefly, 150 uL of the cell media was allowed to bind to the PGE_2 antibody for 1 h at room temperature on a horizontal orbital shaker. During the second incubation (2 h, at room temperature on the horizontal orbital shaker), horseradish peroxidase–labeled PGE_2 was added to bind to the remaining antibody sites. After the wells were aspirated and washed thoroughly, the enzyme-substrate solution was added. Subsequently, the color development was stopped, and the absorbance was read at 450 nm using a spectrophotometer, with intensity inversely proportional to the concentration of PGE_2 in the sample. Each group contained $n = 3$ samples. PGE_2 was normalized to live cells. Three distinct experiments were carried out separately and combined to calculate the mean of each experimental condition.

Statistical Analysis

To analyze Alizarin Red staining, a one-way analysis of variance (ANOVA) was used with a Tukey-HSD post hoc test with statistical significance between each group at $p < 0.05$

($n = 4$). For COX-2 and PGE_2, three hydrogels were combined from three biological repeats. ANOVA followed by Tukey-HSD post hoc tests were performed on all data sets. Statistical significance was indicated by *, corresponding to $p < 0.05$ (n=3).

Results

Effect of Alginate Concentration on Hydrogel Stiffness

Figure 2A shows representative macroscopic images of some of the alginate hydrogels of varying stiffness, and Fig. 2B shows the homogeneity of the same hydrogels through a light microscope. Increasing alginate concentration improved the stability and shape of the hydrogels. The 0.25% alginate hydrogels, for instance, appeared softer and were not homogenous throughout the structure compared to the 1% alginate hydrogels, which seemed more rigid and held their shape and structure. The 0.5% alginate hydrogels were found to have better structural stability for handling than the 0.25% gels and were less stiff than the 1% hydrogels. Alginate hydrogels for rheology studies did not have any peptide coupling as it has been shown that the presence of RGD does not affect the mechanical properties of the hydrogels [30]. Figure 3A shows the storage and loss modulus of the hydrogels with a constant concentration of alginate (2%) and increasing concentrations of the cross-linking agent $CaCl_2$ (2, 5, 10 mM), which resulted in an increase in storage modulus from 500 to 14,000 Pa. Figure 3B shows the same data with a constant concentration of $CaCl_2$ (10 mM) and increasing concentrations of alginate (0.25–2%), which resulted in an increase in storage modulus across a similar range of properties (from 700 to 14,500 Pa), suggesting that the same mechanical stiffness can be achieved via different methods. Other studies have confirmed similar moduli using similar alginate and $CaCl_2$ concentrations [30].

Effect of Alginate Concentration on Cell Viability

Harvested BMSCs showed positive for surface markers ($CD90^+$, $CD105^+$, $CD44^+$, $CD73^+$) through flow cytometry histograms (Fig. 4A and B), confirming their stemness. Qualitative analysis of cell viability in the alginate hydrogels revealed a correlation between stiffness and cell response. Cell morphology was more spread on day 5 in the lower concentration hydrogels (0.25%), more like that seen in cells seeded on TCP, while the cells seeded in 1% hydrogels failed to spread out and were more rounded.

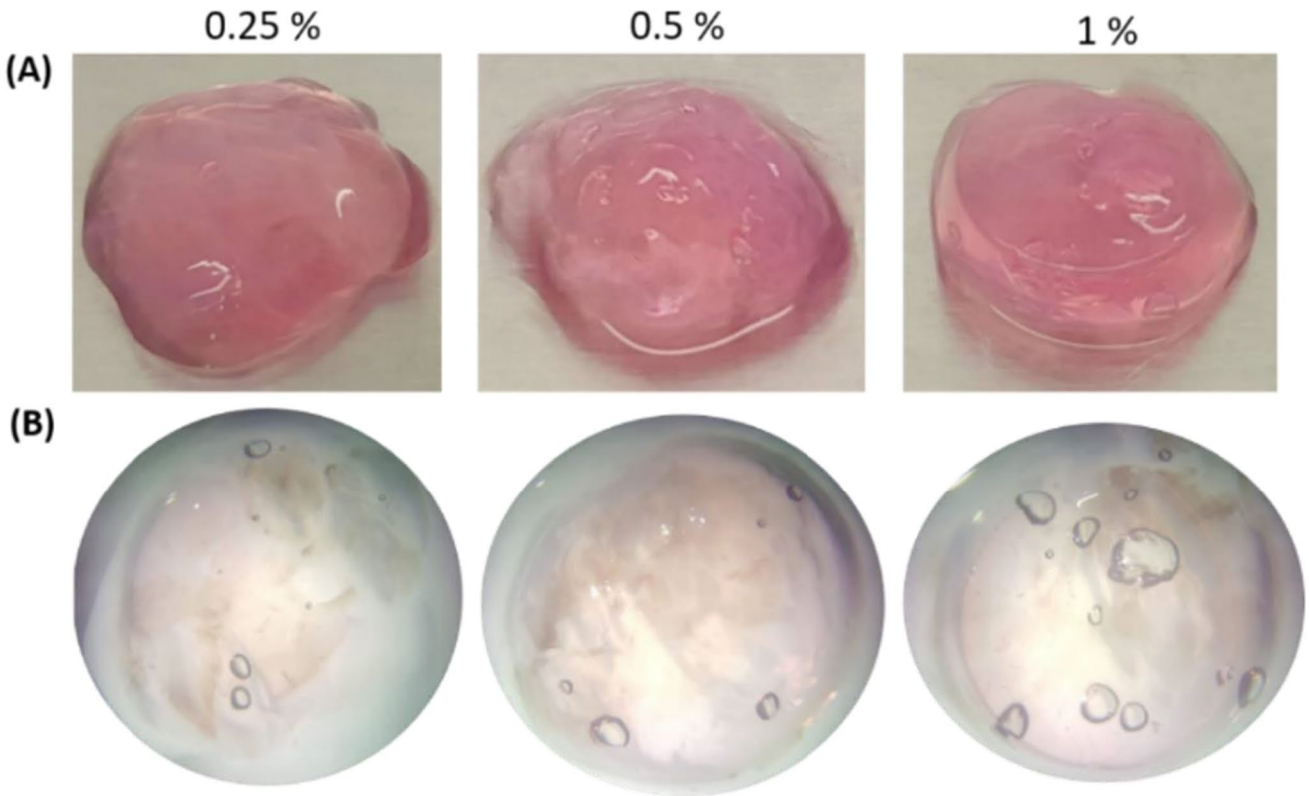

Fig. 2 **A** Macroscopic images of peptide-coupled alginate hydrogels of varying concentrations. **B** Homogeneity of the different alginate hydrogels. The 0.25% alginate hydrogels appeared flaky and inhomogeneous, whereas the 1% alginate hydrogels were stable and maintained shape

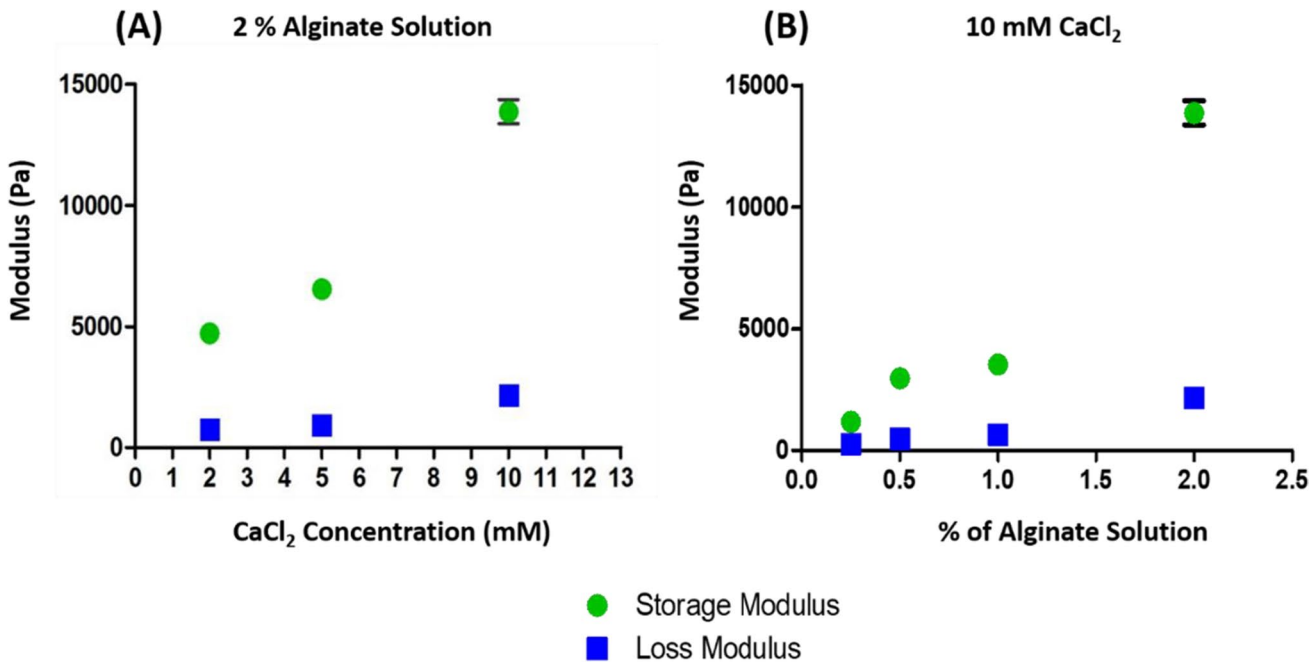

Fig. 3 **A** Rheology data showing the storage and loss modulus of 2% alginate with varying concentrations of $CaCl_2$. Both storage and loss modulus increase with increasing concentration of $CaCl_2$ showing that increased ionic cross-linking within the alginate solution makes stiffer hydrogels. **B** Storage and loss modulus of varying alginate solution with 10 mM $CaCl_2$. Both the storage and loss modulus increase with an increase in the concentration of alginate solution

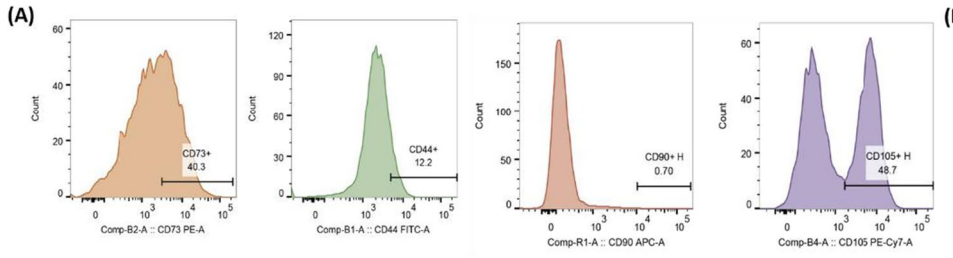

(B)

Stem Cell Marker	% of cells
CD44+	11.9
CD73+	39.07
CD44+ CD73+	83.5
CD90+	0.9
CD105+	49.9

Fig. 4 **A** Flow cytometry histograms for known BMSCs surface markers (CD90+, CD105+, CD44+, CD73+). **B** Marker population reveals that adherent BMSCs express characteristic stem cell markers with 83.5% of cells expressing a double positive marker of CD44+ and CD73+

This correlated with a decrease in cell viability as hydrogel concentration increased, with proliferation dropping after day 5 in the stiffest hydrogels (Fig. 5A). Live/Dead assay (Fig. 5B) corroborated MTS quantitative data (on day 5), showing far fewer live cells in the 1% hydrogels when compared to either 0.25% hydrogels or those on TCP. Given this data and the mechanical analysis, the 0.5% concentration of alginate was determined to be the most promising and was the choice for all subsequent experiments. Ongoing studies are evaluating the impact of both ultrasound and hydrogel degradation over time on cell viability and other markers of cell behavior.

Effect of ARF Intensity on Mineral Formation Within Hydrogels

Figure 6A–E show the macroscopic images of the BMSC-encapsulated 0.5% alginate hydrogels, treated with or without varying ARF intensities. Qualitative analysis of the stained hydrogels revealed the formation of the mineralized matrix throughout the hydrogels. Quantifying the mineralization by measuring the optical density of the desorbed stain showed enhanced mineralization for both 100 and 300 mW/cm^2 groups over the control (Fig. 6F) with a significant increase in the 300 mW/cm^2-treated hydrogels. Interestingly, the alginate hydrogels showed a dip in the mineral formation

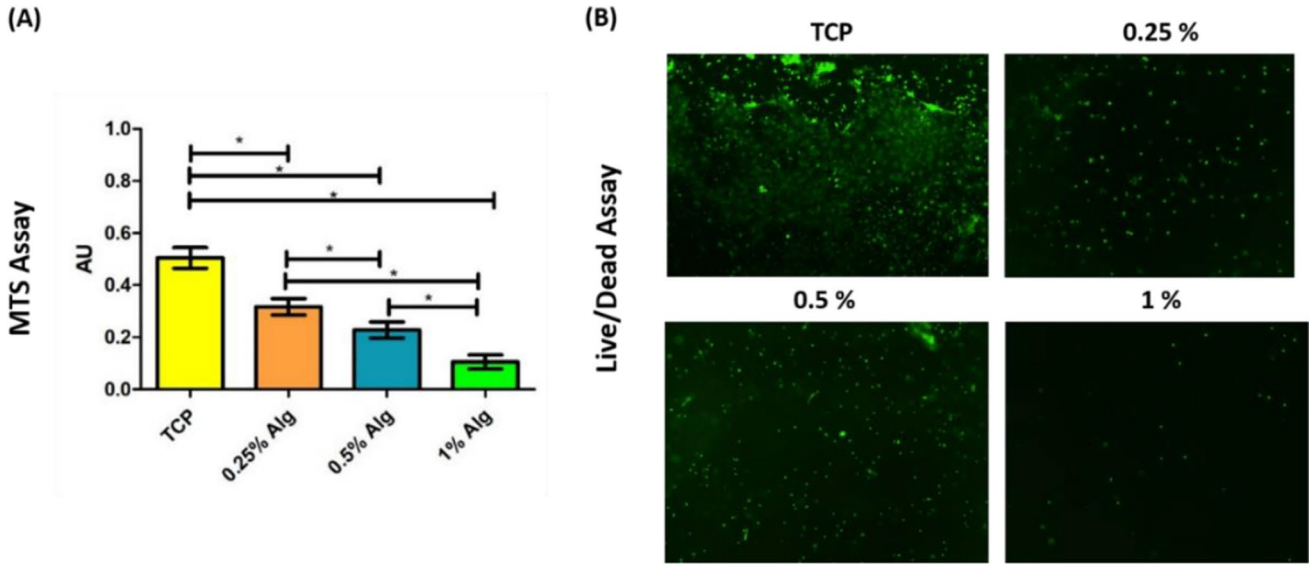

Fig. 5 **A** Quantification of cell viability/proliferation of BMSCs on TCP and in alginate hydrogels of varying concentrations on day 5. **B** Live/Dead assay showing cell morphology. Statistical significance noted (*$P < 0.05$) ($n = 3$). Data shows mean with SD

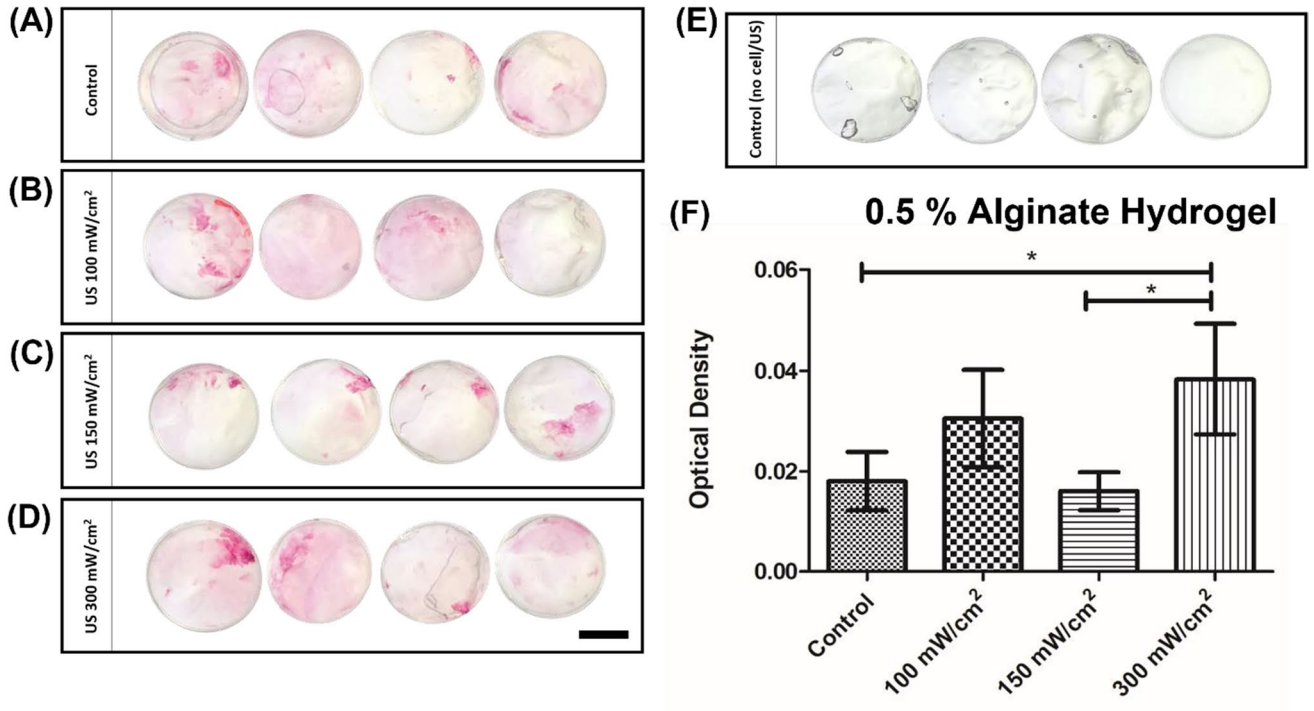

Fig. 6 Mineralization (stained with Alizarin Red) of encapsulated BMSC in 0.5% alginate hydrogels with and without ultrasound treatment on day 21. BMSC-encapsulated 0.5% alginate hydrogels without ultrasound treatment served as the control. **A** The control groups demonstrated sporadic positive Alizarin Red stain. BMSC-encapsulated in 0.5% alginate hydrogels treated with **B** 100 mW/cm^2, **C** 150 mW/cm^2, **D** 300 mW/cm^2. **E** Alizarin Red–stained 0.5% alginate hydrogels alone (neither cells nor ultrasound). Scale bar represents 6 mm. The cell-laden hydrogels treated with the various intensities of ultrasound demonstrated varying amounts of the mineralized matrix within each ultrasound-treated group and across the ultrasound intensities. **F** Optical density quantification of the ARS extracted with CPC ($n = 4$). Graphs show the mean ± SD. A statistically significant increase in mineralized matrix was observed in the 300 mW/cm^2 group compared to the control (*$P < 0.05$)

when exposed to 150 mW/cm^2 intensity, suggesting that the response of the cells was not necessarily correlated with the intensity of the ARF, but rather an indication that certain frequencies may stimulate cells in ways that other frequencies do not. Given that the combination of 0.5% alginate and 300 mW/cm^2 ARF intensity enhanced mineralization significantly over the control, we chose this combination moving forward.

Effect of ARF on Intracellular Calcium Influx

Figure 7 shows the $[Ca^{2+}]_i$ for cells both on and encapsulated within the hydrogels. Representative fluorescent images for cells in each condition (dotted outline) before, during, and after the ARF exposure are shown in Fig. 7A, while Fig. 7B shows the corresponding intensity quantification for the highlighted region. BMSCs seeded on the surface of the hydrogel responded minimally to the ARF and experienced bleaching of the Fluo-4 AM dye towards the end of the data collection. Cells encapsulated in the hydrogel, however, showed an upregulation, as seen in Fig. 7B. It is important to note that while very effort was made to find ROIs that included cells that responded with a change in $[Ca^{2+}]_i$ not every cell that was exposed to ARF responded equally, a phenomenon seen in other studies that have evaluated $[Ca^{2+}]_i$ after mechanical loading [31]. Figure 7C shows the representative relative fluorescent intensities for three different cells across ten different experiments. This data, when compared to cells on TCP (data not shown), suggests that encapsulating the cells within the hydrogel may minimally mute the cellular response that is seen from cells on a rigid substrate but certainly does not eliminate it, which stands in contrast to cells that were seeded on top of the hydrogel that showed very little if any $[Ca^{2+}]_i$.

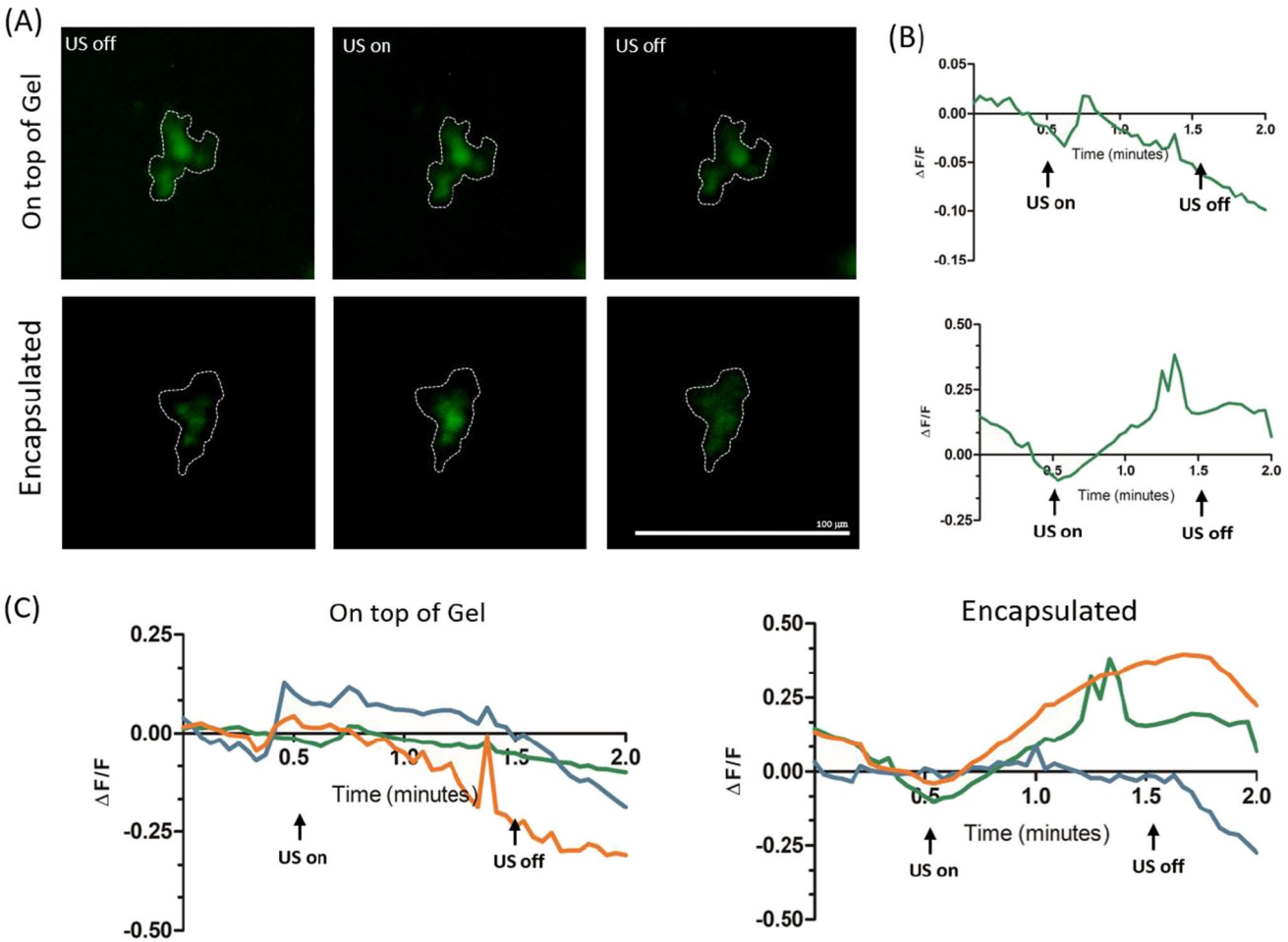

Fig. 7 Calcium influx of BMSCs on the surface of and encapsulated in 0.5% alginate hydrogel during the exposure to 300 mW/cm^2 ultrasound intensity. **A** Representative fluorescent image of cells (outlined) within a region showing the fluorescence intensity during the exposure. **B** Relative intensity quantification of the outlined regions. **C** The relative intensity of individual cells across experiments shows the calcium influx within cells ($n = 3$). For cells on top of the hydrogel, no noticeable change in calcium influx was observed. For encapsulated cells, during the initial 30-s period, when ultrasound was OFF, no calcium influx was visible, but at the onset of the ultrasound signal, the calcium influx was enhanced in cells and gradually decayed when the ultrasound was OFF again

Effect of ARF on COX-2 and PGE_2 Upregulation

COX-2 and PGE_2 expression was measured in ARF-stimulated BMSCs shortly after exposure, as their expression can be transient and short-lasting. The goal was to study how a one-time ARF exposure of 20 min to the cell-encapsulated hydrogels affects this transient expression of these markers. BMSCs that were encapsulated in 0.5% alginate hydrogels were subject to a one-time, 20-min ARF application at an intensity of 300 mW/cm^2. COX-2 expression was enhanced after ARF exposure in the encapsulated cells over those not receiving ARF, but not with statistical significance (Fig. 8A). Cell encapsulation alone, within hydrogels of varying stiffness, increased the COX-2 expression (Supplementary Data). As Supplementary Fig. I demonstrates, increasing hydrogel stiffness from the 0.25% hydrogels to the 0.5% hydrogels also increased the COX-2 expression significantly. This demonstrates that the stiffness of the encapsulating material around the cells alone played a role in enhancing the COX-2 expression.

PGE_2 expression was also upregulated after ARF exposure, but this time with statistical significance (Fig. 8B). PGE_2 levels across all groups were enhanced just with the presence of the hydrogel. When the stiffness of the hydrogels increased, the cells produced more PGE_2, which suggested that matrix stiffness affects both COX-2 and PGE_2 levels (Supplementary Fig. I).

Discussion

Mechanical Properties of Alginate Hydrogels

A few studies have described how ultrasound impacts alginate hydrogels, both with and without encapsulated cells. One study that combined alginate hydrogels with ultrasound exposure showed that an acoustic pressure of around 85 kPa changed the physical properties of the hydrogel, specifically the porosity and permeability, by generating microbubbles (cavitation) that propagated through the matrix and induced shear stress. It was believed that this stress caused the pores within the alginate hydrogels to interconnect and stimulate enhanced cell growth [32, 33]. We have not observed any changes to bulk mechanical properties as a result of ARS alone (unpublished data) and continue to examine the relationship between the two. Wang et al. [9] thought that ultrasound applied to hMSCs encapsulated in alginate/chitosan hydrogels altered the permeability of the cell membrane, and lead to an enhanced role of cytokines and RGD towards osteogenesis. Other studies have focused on the cavitation

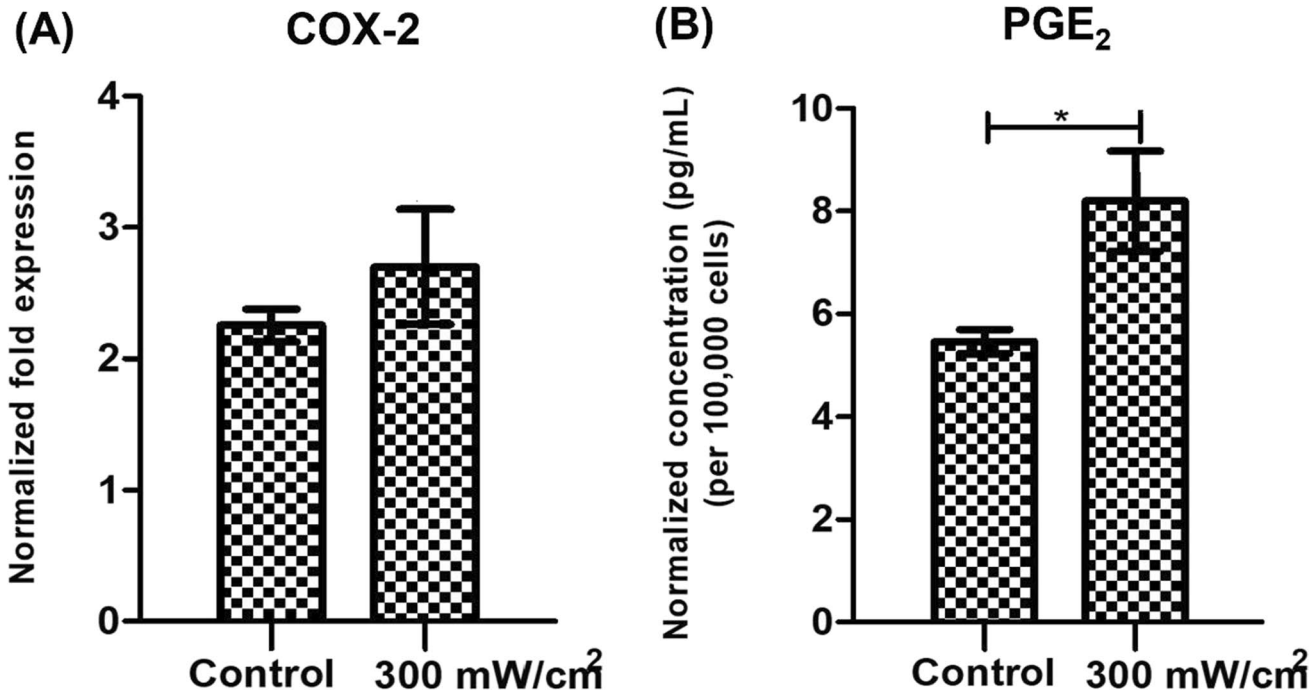

Fig. 8 The COX-2 and the PGE_2 quantification of 0.5% alginate hydrogels exposed to a one-time ultrasound exposure of 300 mW/cm^2 spatial intensity. **A** COX-2 gene expression was quantified through RT-PCR. Ultrasound treatment of BMSCs encapsulated in 0.5% alginate hydrogel enhanced COX-2 expression over the control, although not significantly. **B** Normalized PGE_2 expression per 100,000 cells quantified through ELISA. PGE_2 expression was significantly upregulated in 0.5% hydrogels when treated with ultrasound compared to the control groups. Error is reported in bar graphs as the standard deviation of the mean. Statistical significance noted (*$P < 0.05$) ($n = 3$)

phenomenon, but none has examined how mechanically deforming the hydrogel, as in our studies, influences encapsulated stem cell behavior. In our studies, we evaluated a range of alginate concentrations to see how the concentration impacted stiffness and usability. Figure 2 shows macroscopic images of alginate hydrogels with 0.25, 0.5, and 1% alginate and reveals that the lowest concentration of alginate was unable to maintain its short cylindrical shape under its own weight, which would be problematic in clinical applications. The other two concentrations, 0.5 and 1%, allowed for the shape to be retained. Handling these was easier as well, as they were stiff enough to have some mechanical integrity. The importance of being able to physically handle these hydrogels and have them maintain their shape when moved around is less apparent on the laboratory benchtop but it becomes more important when one considers the translation of this to the clinical bedside where surgeons may be placing them into defects and would need to be able to manipulate them into place without them falling apart.

Cell Viability in Varying Stiffness of Alginate Hydrogels

It has been well-documented in the literature that cells generally spread, attach, and proliferate readily on 2-dimensional, rigid substrates like TCP [25, 26, 34, 35]. On the other hand, 3-dimensional culture, which more accurately recapitulates the native tissue environment, causes cells to adopt a different morphology and in some cases can restrict cell spreading and migration [36] and can even impact cell viability. This may be due to the density of matrix cross-linking surrounding the cells [34, 36], and is an important consideration when developing a 3-D culture environment. Proliferation studies described here revealed lower cell survival in the 1% alginate hydrogels than in lower concentrations, and cells failed to fully spread out in the 3-D space, possibly due to the cross-linking density. Alginate hydrogels alone do not have a cell adhesion motif and would not support cell proliferation as is, but they can be modified by incorporating the peptide sequence (RGD) into the alginate monomers to improve cell adhesion and viability without affecting mechanical properties [30, 37–39]. For these studies, alginate was purchased with the RGD-peptide sequence already incorporated so any matrix influence on proliferation was most likely due to cross-linking density. Interestingly, the 0.25% concentration of alginate resulted in a hydrogel with so little alginate that it was too soft and unable to maintain its shape under its own weight, so accurate proliferation was difficult to measure. For these reasons, the 0.25% and 1% concentrations were deemed unsuitable for further study and the 0.5% hydrogel was chosen as optimal for structural stability and cell viability.

Mineralization Studies

The most critical aspect of this work is demonstrating the ability to form bone within the hydrogel. The choice of hydrogel material, stiffness, and ARF intensity are all based on how they work together to support cell-based mineralization. While the other parameters are necessary and serve to inform the overall design of this system, the *sine qua non* is mineralization and without mineralization there is no bone repair. In these studies, the 0.5% alginate hydrogels demonstrated an increase in mineralization (as indicated by ARS quantification) for two of the three different ARF intensities tested, compared to the control group that received no ultrasound treatment. Groups treated with 300 mW/cm^2 intensity increased mineralization compared to the control ($p<0.05$) while the increase seen with 100mW/cm^2 over the control was not statistically significant. Interestingly, the 150mW/cm^2 intensity had no effect on mineralization at all. This indicates that mineralization is not directly correlated to ARF intensity, but that greater intensities, which cause greater hydrogel deformation and force magnitude applied to cells, do cause more mineralization. This increased physical force on encapsulated BMSCs may result in loading similar to fluid shear or drag forces around the cells that have been shown to stimulate matrix mineralization in other studies [40–42]. Thus, there is an optimal loading condition that is modulated by both stiffness and intensity.

Calcium Ion Signaling

Osteoblasts have several voltage-gated and mechanosensitive channels on the surface that are activated in response to physical forces. Mechanical stimulation through ultrasound or fluid flow can activate hemichannels, Gd3+ sensitive stretch-activated ion channels, and gap junctions [43–45]. The activation of these channels permits both the influx of calcium ions and in some cases the liberation of intracellular stores, each of which has been linked to the function of bone cells. For instance, Hung et al. [43] suggested that both extracellular calcium signaling through ion channels and inositol 1,4,5-trisphosphate (IP_3)–induced intracellular calcium signaling (where calcium is released from the intracellular stores) are required to produce calcium cell signaling in bone cells in response to fluid flow. Li et al. [46] and Jacobs et al [47] demonstrated that BMSCs subjected to oscillatory fluid flow (OFF) in a parallel plate flow chamber responded with an increase in intracellular calcium concentration, enhanced proliferation, and upregulation in osteoblastic gene expression, which indicated that calcium upregulation early on in the study resulted in a cascade of downstream signaling pathways. It was also shown that an increase in intracellular $[Ca^{2+}]_i$ is an immediate response of rat MSCs in response to fluid shear stress (FSS) and that

calcium is one of the key molecules in the mechanotransduction of MSCs and its intracellular response to changes in mechanical stresses [48].

In our studies, calcium influx was noted immediately after the onset of ultrasound when cells were encapsulated in the hydrogel compared to the cells seeded on top of the gels. This shows that the presence of the hydrogel around the cells altered the way the cells perceived and responded to the ultrasound forces, possibly because the physical forces from the ARF deform the gel that may, in turn, produce additional mechanical loading, similar to fluid or drag forces around encapsulated cells. The volume of hydrogel used for calcium ion imaging studies was less than that used in other studies, but was still much larger in volume than the encapsulated cells, and therefore was still an accurate representation of how the cells in a gel respond differently than those on top of the gel. Campbell et al. [31] measured the frequency of intracellular calcium of human MSCs encapsulated in alginate constructs under static compressive strain and observed a similar response to ours. In our studies, the most likely explanation for the intracellular calcium upregulation would be the activation of stretch-activated ion channels by the ultrasound-derived matrix deformation. More detailed experiments using pharmaceutical blockers or chelators would elucidate which signaling pathway and/or specific channels were more prone to respond to ultrasound-triggered physical forces for encapsulated cells.

COX-2 and PGE_2 Production

Bone cells have been shown to respond to both pulsatile fluid flow (PFF) and cyclic strain with an increase in COX-2 and PGE_2 production [24, 49–51]. Mullender et al. [52] exposed primary bone cells that were harvested from human bone fragments to either PFF or cyclic strain and noted an increase in PGE_2 expression and matrix production, respectively. Studies by You et al. [40], Orr et al. [41], and Chen et al. [42] have suggested a possible link between the forces that these flows produce and the drag forces and fluid flow within the canaliculi and pericellular spaces of bone, and suggest that they can have a significant influence on the cellular responses within a bone. This concept is potentially applicable to systems like the one described here and others that use ultrasound as the source of mechanical force. It is our belief that the ultrasound-derived deformation of the cell-laden hydrogel is similar to the fluid-derived drag forces of bone, perhaps loading the cells in a similar fashion. In fact, other systems that use ultrasound directly on cells (i.e., not encapsulated) have reported results similar to those found here. Kokubu et al. [53] for instance showed that ultrasound modulated the production of PGE_2 via the expression of COX-2 in a manner similar to fluid shear stress and tensile forces. Li et al. [54] studied the optimal ultrasound intensity for PGE_2 secretion in osteoblasts and found that an intensity of 600 mW/cm^2 enhanced both cell proliferation and PGE_2 production. Other studies have shown that ultrasound not only enhanced the production of PGE_2 but also stimulated new vasculature, increased collagen synthesis, enhanced proliferation of osteoblasts, increased calcification in the matrix, and stimulated bone resorption at the fracture site [55–61].

The results of our work parallel the published literature in that COX-2 and PGE_2 expression increased as a result of the ultrasound (PGE_2 significantly increased). Importantly, this expected upregulation was not diminished by encapsulating the cells in hydrogels. Interestingly, the hydrogels themselves may have contributed to the upregulation in expression since just changing the stiffness of the hydrogel (from 0.25 to 0.5%) without adding ultrasound had a measurable effect on both COX-2 expression and PGE_2 production of BMSCs (Supplemental Fig. 1). Encapsulating the cells within a 3D matrix does change the mechanical environment of the cells considerably compared to 2D culture on TCP so this may have been a response to that. The 3D matrix can also contribute by influencing cell morphology, which is quite different on 2D surfaces versus 3D cultures [20, 25, 62]. Similar work has shown that cells respond to significantly lower shear stresses when grown in 3D environments compared to 2D surfaces [63–65] further supporting that mechanical loading in a 3D culture is quite different mechanically than cells in 2D cultures [20, 65, 66].

Conclusions

Here, we described a system of blending cell therapy with low-intensity acoustic radiation force to apply a mechanical load to BMSCs encapsulated in alginate hydrogels. The benefit of this approach comes in the ability to implant a cell-laden, cross-linked alginate hydrogel of a desired stiffness into a bone defect, close the surgical site to allow the healing process to begin, and periodically provide mechanical stimulation to the hydrogel-filled bone defect transdermally. This transdermal stimulation will provide therapeutic mechanical stimulation to the encapsulated stem cells without destabilizing the injury site, something that is impossible using other methods of mechanical loading. For use in the clinical field, BMSCs could be harvested from the donor, grown in culture, and then encapsulated in such alginate hydrogels via the method described here and then placed surgically into the bone defect. Our previous studies revealed the efficacy of this approach using collagen hydrogels, and through the studies conducted in this work, we can conclude that alginate hydrogels are also a potential hydrogel platform that represents a wider range of mechanical properties and demonstrates that the success of this approach is not tied to any

specific hydrogel system. Results show that cells respond to both hydrogel stiffness and the radiation force intensity with increased calcium ion mobilization in encapsulated cells and COX-2 and PGE_2 expression increases, resulting in more mineralized tissue formation This data demonstrates the potential of this approach as a novel treatment for large-scale bone defects and that alginate hydrogels provide another platform towards this cell therapy approach.

Future Works Future studies will include evaluating this technique using in vivo bone repair models in both cortical and trabecular bone defects and expanding this technique to other hydrogel systems to show its application across different material platforms.

Supplementary Information The online version contains supplementary material available at https://doi.org/10.1007/s40883-023-00312-2.

Acknowledgements The content is solely the responsibility of the authors and does not necessarily represent the official views of the National Institutes of Health.

Author Contribution Conceptualization: Y. K., F. A. Experimental design: Y. K., F. A., H. A., K. G., L. N. Experimental work: F. A., H. A., K. G. Manuscript preparation, writing, and editing: Y. K., F. A., L. N. Final approval of manuscript: F. A., Y. K., K. G., H. A., L. N.

Funding Research reported in this publication was wholly supported by the National Science Foundation under award #1752915 and the National Institute of Arthritis and Musculoskeletal and Skin Diseases of the National Institutes of Health under award number R01AR073206.

Declarations

Conflict of Interest The authors declare no competing interests.

References

1. Meinel L, Karageorgiou V, Fajardo R, Snyder B, Shinde-Patil V, Zichner L, Kaplan D, Langer R, Vunjak-Novakovic G. Bone tissue engineering using human mesenchymal stem cells: effects of scaffold material and medium flow. Ann Biomed Eng. 2004;32(1):112–22.
2. Amini AR, Laurencin CT, Nukavarapu SP. Bone tissue engineering: recent advances and challenges. Crit Rev Biomed Eng. 2012;40(5):363–408.
3. Murphy MP, Quarto N, Longaker MT, Wan DC. (*) Calvarial defects: cell-based reconstructive strategies in the murine model. Tissue Eng Part C Methods. 2017;23(12):971–81.
4. Stewart S, Bryant SJ, Ahn J, Hankenson KD. Chapter 24 - Bone regeneration. In: Atala A, Allickson JG, editors. Translational Regenerative Medicine. Boston: Academic Press; 2015. p. 313–33.
5. Zimmermann G, Moghaddam A. Allograft bone matrix versus synthetic bone graft substitutes. Injury. 2011;42(Suppl 2):S16–21.
6. Parikh SN. Bone graft substitutes: past, present, future. J Postgrad Med. 2002;48(2):142–8.
7. Ibrahim A. 13 - 3D bioprinting bone. In: Thomas DJ, Jessop ZM, Whitaker IS, editors. 3D Bioprinting for Reconstructive Surgery. Woodhead Publishing; 2018. p. 245–75.
8. He R, Chen J, Jiang J, Liu B, Liang D, Zhou W, Chen W, Wang Y. Synergies of accelerating differentiation of bone marrow mesenchymal stem cells induced by low intensity pulsed ultrasound, osteogenic and endothelial inductive agent, Artif. Cells, Nanomed. Biotechnol. 2019;47(1):673–83.
9. Wang Y, Peng W, Liu X, Zhu M, Sun T, Peng Q, Zeng Y, Feng B, Zhi W, Weng J, Wang J. Study of bilineage differentiation of human-bone-marrow-derived mesenchymal stem cells in oxidized sodium alginate/N-succinyl chitosan hydrogels and synergistic effects of RGD modification and low-intensity pulsed ultrasound. Acta Biomater. 2014;10(6):2518–28.
10. Nguyen B-NB, Moriarty RA, Kamalitdinov T, Etheridge JM, Fisher JP. Collagen hydrogel scaffold promotes mesenchymal stem cell and endothelial cell coculture for bone tissue engineering. J Biomed Mater Res A. 2017;105(4):1123–31.
11. Zhou X, Castro NJ, Zhu W, Cui H, Aliabouzar M, Sarkar K, Zhang LG. Improved human bone marrow mesenchymal stem cell osteogenesis in 3D bioprinted tissue scaffolds with low intensity pulsed ultrasound stimulation. Sci Rep. 2016;6(1):32876.
12. Maisani M, Ziane S, Ehret C, Levesque L, Siadous R, Le Meins J-F, Chevallier P, Barthélémy P, De Oliveira H, Amédée J, Mantovani D, Chassande O. A new composite hydrogel combining the biological properties of collagen with the mechanical properties of a supramolecular scaffold for bone tissue engineering. J Tissue Eng Regen Med. 2018;12(3):e1489–500.
13. Roseti L, Parisi V, Petretta M, Cavallo C, Desando G, Bartolotti I, Grigolo B. Scaffolds for bone tissue engineering: state of the art and new perspectives. Mater Sci Eng C. 2017;78:1246–62.
14. Liu M, Zeng X, Ma C, Yi H, Ali Z, Mou X, Li S, Deng Y, He N. Injectable hydrogels for cartilage and bone tissue engineering. Bone Research. 2017;5(1):17014.
15. Arrighi N. 3 - Stem cells at the core of cell therapy. In: Arrighi N, editor. Stem Cells. Elsevier; 2018. p. 73–100.
16. Carson CT, Emre N, McIntyre C, Fong TC. 3.36 - Cellular therapies. In: Moo-Young M, editor. Comprehensive Biotechnology (Third Edition). Oxford: Pergamon; 2011. p. 446–59.
17. Rothrauff BB, Pirosa A, Lin H, Sohn J, Langhans MT, Tuan RS. Chapter 54 - Stem cell therapy for musculoskeletal diseases. In: Atala A, Lanza R, Mikos AG, Nerem R, editors. Principles of Regenerative Medicine (Third Edition). Boston: Academic Press; 2019. p. 953–70.
18. Veronick J, Assanah F, Nair LS, Vyas V, Huey B, Khan Y. The effect of acoustic radiation force on osteoblasts in cell/hydrogel constructs for bone repair. Exp Biol Med. 2016;241(10):1149–56.
19. Veronick JA, Assanah F, Piscopo N, Kutes Y, Vyas V, Nair LS, Huey BD, Khan Y. Mechanically loading cell/hydrogel constructs with low-intensity pulsed ultrasound for bone repair. Tissue Eng Part A. 2018;24(3-4):254–63.
20. Assanah F, Khan Y. Cell responses to physical forces, and how they inform the design of tissue-engineered constructs for bone repair: a review. J Mater Sci. 2018;53(8):5618–40.
21. Lee DA, Knight MM, Campbell JJ, Bader DL. Stem cell mechanobiology. J Cell Biochem. 2011;112(1):1–9.
22. MacQueen L, Sun Y, Simmons CA. Mesenchymal stem cell mechanobiology and emerging experimental platforms. J R Soc Interface. 2013;10(84):20130179.
23. Huang CH, Chen MH, Young TH, Jeng JH, Chen YJ. Interactive effects of mechanical stretching and extracellular matrix proteins on initiating osteogenic differentiation of human mesenchymal stem cells. J Cell Biochem. 2009;108(6):1263–73.
24. Klein-Nulend J, Burger EH, Semeins CM, Raisz LG, Pilbeam CC. Pulsating fluid flow stimulates prostaglandin release and inducible

prostaglandin G/H synthase mRNA expression in primary mouse bone cells. J Bone Miner Res. 1997;12(1):45–51.
25. Engler AJ, Sen S, Sweeney HL, Discher DE. Matrix elasticity directs stem cell lineage specification. Cell. 2006;126(4):677–89.
26. Sun M, Chi G, Li P, Lv S, Xu J, Xu Z, Xia Y, Tan Y, Xu J, Li L, Li Y. Effects of matrix stiffness on the morphology, adhesion, proliferation and osteogenic differentiation of mesenchymal stem cells. Int J Med Sci. 2018;15(3):257–68.
27. Lv H, Li L, Sun M, Zhang Y, Chen L, Rong Y, Li Y. Mechanism of regulation of stem cell differentiation by matrix stiffness. Stem Cell Res Ther. 2015;6(1):103.
28. Pal P, Nguyen QC, Benton AH, Marquart ME, Janorkar AV. Drug-loaded elastin-like polypeptide–collagen hydrogels with high modulus for bone tissue engineering. Macromol Biosci. 2019;19(9):1900142.
29. Assanah F, Grassie K, Anderson H, Xin X, Rowe D, Khan Y. Ultrasound-derived mechanical stimulation of cell-laden collagen hydrogels for bone repair. J Biomed Mater Res A. 2023;111(8):1200–15.
30. Duan P, Kandemir N, Wang J, Chen J. Rheological characterization of alginate based hydrogels for tissue engineering. MRS Advances. 2017;2(24):1309–14.
31. Campbell JJ, Bader DL, Lee DA. Mechanical loading modulates intracellular calcium signaling in human mesenchymal stem cells. J Appl Biomater Biomech. 2008;6(1):9–15.
32. Guo G, Ma Y, Guo Y, Zhang C, Guo X, Tu J, Yu ACH, Wu J, Zhang D. Enhanced porosity and permeability of three-dimensional alginate scaffolds via acoustic microstreaming induced by low-intensity pulsed ultrasound. Ultrason Sonochem. 2017;37:279–85.
33. Guo G, Lu L, Ji H, Ma Y, Dong R, Tu J, Guo X, Qiu Y, Wu J, Zhang D. Low intensity pulse ultrasound stimulate chondrocytes growth in a 3-D alginate scaffold through improved porosity and permeability. Ultrasonics. 2015;58:43–52.
34. Lutolf MP, Lauer-Fields JL, Schmoekel HG, Metters AT, Weber FE, Fields GB, Hubbell JA. Synthetic matrix metalloproteinase-sensitive hydrogels for the conduction of tissue regeneration: engineering cell-invasion characteristics. Proc Natl Acad Sci. 2003;100(9):5413–8.
35. Wells R. The role of matrix stiffness in regulating cell behavior. Hepatology. 2008;47:1394–400.
36. Bott K, Upton Z, Schrobback K, Ehrbar M, Hubbell J, Lutolf M, Rizzi S. The effect of matrix characteristics on fibroblast proliferation in 3D gels. Biomaterials. 2010;31:8454–64.
37. Anamizu M, Tabata Y. Design of injectable hydrogels of gelatin and alginate with ferric ions for cell transplantation. Acta Biomater. 2019;100:184–90.
38. Rowley JA, Madlambayan G, Mooney DJ. Alginate hydrogels as synthetic extracellular matrix materials. Biomaterials. 1999;20(1):45–53.
39. Sarker B, Rompf J, Silva R, Lang N, Detsch R, Kaschta J, Fabry B, Boccaccini AR. Alginate-based hydrogels with improved adhesive properties for cell encapsulation. Int J Biol Macromol. 2015;78:72–8.
40. You L, Cowin SC, Schaffler MB, Weinbaum S. A model for strain amplification in the actin cytoskeleton of osteocytes due to fluid drag on pericellular matrix. J Biomech. 2001;34(11):1375–86.
41. Orr AW, Helmke BP, Blackman BR, Schwartz MA. Mechanisms of mechanotransduction. Dev Cell. 2006;10(1):11–20.
42. Chen T, Buckley M, Cohen I, Bonassar L, Awad HA. Insights into interstitial flow, shear stress, and mass transport effects on ECM heterogeneity in bioreactor-cultivated engineered cartilage hydrogels. Biomech Model Mechanobiol. 2012;11(5):689–702.
43. Hung CT, Allen FD, Pollack SR, Brighton CT. Intracellular Ca2+ stores and extracellular Ca2+ are required in the real-time Ca2+ response of bone cells experiencing fluid flow. J Biomech. 1996;29(11):1411–7.
44. Yoon CW, Jung H, Goo K, Moon S, Koo KM, Lee NS, Weitz AC, Shung KK. Low-intensity ultrasound modulates Ca(2+) dynamics in human mesenchymal stem cells via connexin 43 hemichannel. Ann Biomed Eng. 2018;46(1):48–59.
45. Zhang S, Cheng J, Qin Y-X. Mechanobiological modulation of cytoskeleton and calcium influx in osteoblastic cells by short-term focused acoustic radiation force. PloS One. 2012;7(6):e38343.
46. Li YJ, Batra NN, You L, Meier SC, Coe IA, Yellowley CE, Jacobs CR. Oscillatory fluid flow affects human marrow stromal cell proliferation and differentiation. J Orthop Res. 2004;22(6):1283–9.
47. Jacobs CR, Yellowley CE, Davis BR, Zhou Z, Cimbala JM, Donahue HJ. Differential effect of steady versus oscillating flow on bone cells. J Biomech. 1998;31(11):969–76.
48. Wenfu Z, Xie Y, Zhang W, Wang D, Wanshun M, Wang Z, Jiang X. Fluid flow stress induced contraction and re-spread of mesenchymal stem cells: a microfluidic study. Integr Biol. 2012;4:1102–11.
49. Reich K, Frangos JA. Effect of flow on prostaglandin E2 and inositol trisphosphate levels in osteoblasts. Am J Physiol. 1991;261:C428–32.
50. Nauman E, Satcher R, Keaveny T, Halloran B, Bikle D. Osteoblasts respond to pulsatile fluid flow with short-term increases in PGE2 but no change in mineralization. J Appl Physiol. 1985;90(2001):1849–54.
51. Donahue T, Haut T, Yellowley CE, Donahue H, Jacobs C. Mechanosensitivity of bone cells to oscillating fluid flow induced shear stress may be modulated by chemotransport. J Biomech. 2003;36:1363–71.
52. Mullender M, El Haj AJ, Yang Y, van Duin MA, Burger EH, Klein-Nulend J. Mechanotransduction of bone cellsin vitro: mechanobiology of bone tissue. Med Biol Eng Comput. 2004;42(1):14–21.
53. Kokubu T, Matsui N, Fujioka H, Tsunoda M, Mizuno K. Low intensity pulsed ultrasound exposure increases prostaglandin E2 production via the induction of cyclooxygenase-2 mRNA in mouse osteoblasts. Biochem Biophys Res Commun. 1999;256(2):284–7.
54. Li JG, Chang WH, Lin JC, Sun JS. Optimum intensities of ultrasound for PGE(2) secretion and growth of osteoblasts. Ultrasound Med Biol. 2002;28(5):683–90.
55. Li J, Chang W, Lin C-A, Sun J-S. Optimum intensities of ultrasound for PGE2 secretion and growth of osteoblasts. Ultrasound Med Biol. 2002;28:683–90.
56. Tsai CL, Chang WH, Liu TK, Song GM. Ultrasound can affect bone healing both locally and systemically. Chin J Physiol. 1991;34(2):213–22.
57. Harle J, Salih V, Mayia F, Knowles JC, Olsen I. Effects of ultrasound on the growth and function of bone and periodontal ligament cells in vitro. Ultrasound Med Biol. 2001;27(4):579–86.
58. Yang K-H, Parvizi J, Wang S-J, Lewallen DG, Kinnick RR, Greenleaf JF, Bolander ME. Exposure to low-intensity ultrasound increases aggrecan gene expression in a rat femur fracture model. J Orthop Res. 1996;14(5):802–9.
59. Nagai M, Suzuki Y, Ota M. Systematic assessment of bone resorption, collagen synthesis, and calcification in chick

embryonic calvaria in vitro: effects of prostaglandin E2. Bone. 1993;14(4):655–9.
60. Reher P, Harris M, Whiteman M, Hai HK, Meghji S. Ultrasound stimulates nitric oxide and prostaglandin e2 production by human osteoblasts. Bone. 2002;31(1):236–41.
61. Reher P, Elbeshir E-NI, Harvey W, Meghji S, Harris M. The stimulation of bone formation in vitro by therapeutic ultrasound. Ultrasound Med Biol. 1997;23(8):1251–8.
62. Engler A, Bacakova L, Newman C, Hategan A, Griffin M, Discher D. Substrate compliance versus ligand density in cell on gel responses. Biophys J. 2004;86(1):617–28.
63. Delaine-Smith RM, Reilly GC. Mesenchymal stem cell responses to mechanical stimuli. Muscles, Ligaments Tendons J. 2012;2(3):169–80.
64. Griffith LG, Swartz MA. Capturing complex 3D tissue physiology in vitro. Nat Rev Mol Cell Biol. 2006;7(3):211–24.
65. Zhao F, Chella R, Ma T. Effects of shear stress on 3-D human mesenchymal stem cell construct development in a perfusion bioreactor system: experiments and hydrodynamic modeling. Biotechnol Bioeng. 2007;96(3):584–95.
66. McCoy RJ, O'Brien FJ. Influence of shear stress in perfusion bioreactor cultures for the development of three-dimensional bone tissue constructs: a review. Tissue Eng Part B Rev. 2010;16(6):587–601.